Improving LiDAR height precision in urban environment

Low-cost GNSS ranging prototype for post-mission airborne laser scanning enhancement

Salehi-Dorcheabedi, Milad; Asgari, Jamal; Amiri-Simkooei, Alireza; Fatemi Nasrabadi, Sayyed Bagher

DOI
10.1016/j.rsase.2024.101251

Publication date
2024

Document Version
Final published version

Published in
Remote Sensing Applications: Society and Environment

Remote Sensing Applications: Society and Environment 35 (2024) 101251

Contents lists available at ScienceDirect

Remote Sensing Applications: Society and Environment

journal homepage: www.elsevier.com/locate/rsase

Improving LiDAR height precision in urban environment: Low-cost GNSS ranging prototype for post-mission airborne laser scanning enhancement

Milad Salehi-Dorcheabedi [a], Jamal Asgari [a, *], Alireza Amiri-Simkooei [a, b], Sayyed Bagher Fatemi Nasrabadi [a]

[a] Department of Geomatics Engineering, Faculty of Civil Engineering and Transportation, University of Isfahan, Isfahan, 81746-73441, Iran
[b] Department of Control and Operations, Faculty of Aerospace Engineering, Delft University of Technology, Delft, the Netherlands

ARTICLE INFO

Keywords:
Light detection and ranging (LiDAR)
Airborne laser scanning system accuracy assessment
Global navigation satellite system (GNSS)
Network real time kinematic (NRTK)
Ultrasonic distance measuring

ABSTRACT

Although Light Detection and Ranging (LiDAR) technology is currently one of the most efficient methods for acquiring high-density point cloud, there are still challenges in terms of data reliability. In particular, the accuracy assessment of LiDAR data, especially in the height component, is one of the main issues in this context. This study introduces a rapid and cost-effective platform to improve the accuracy and precision of LiDAR data by integrating high-density GNSS-Ranging measurements with LiDAR data. The platform offers the capability to rapidly collect a significant number of network real time kinematic (NRTK) points with centimetric precision. A continuous correction surface is proposed to integrate the platform and LiDAR data, resulting in improved accuracy for all ground-class LiDAR data. Evaluation using GNSS benchmarks and NRTK checkpoints showed a significant reduction in LiDAR height errors after applying the correction surface. The root mean squares error (RMSE) decreased from 18.5 cm to 8.2 cm when compared to GNSS benchmarks and from 17.4 cm to 5.3 cm for approximately 1000 NRTK control points. The results indicate that collecting a large number of high-density GNSS ground targets and applying a correction surface to LiDAR height data significantly enhance the accuracy and precision of the LiDAR extracted products.

1. Introduction

Airborne LiDAR, also known as airborne laser scanning (ALS), has been a well-known active remote sensing method for collecting 3D geospatial data since the emergence of laser scanning in the early 1990s. Applications of the LiDAR technology are rapidly expanding in space science and geomatics engineering. An important application of this technique is the production of three-dimensional ground data, especially digital height data, which is easier and less expensive than the traditional mapping techniques. As a result, this method is currently widely used as a state-of-the-art technology for various surface modeling (Vo et al., 2016; Dong and Chen, 2017).

* Corresponding author.
E-mail addresses: mi.salehi@eng.ui.ac.ir (M. Salehi-Dorcheabedi), asgari@eng.ui.ac.ir (J. Asgari), a.amirisimkooei@tudelft.nl (A. Amiri-Simkooei), sb.fatemi@eng.ui.ac.ir (S.B. Fatemi Nasrabadi).

https://doi.org/10.1016/j.rsase.2024.101251
Received 9 March 2024; Received in revised form 2 May 2024; Accepted 21 May 2024
Available online 22 May 2024

1.1. Background

The airborne LiDAR equipment sends laser light pulses toward a target object and receives the light reflected by this object (Favorskaya and Jain, 2017). An aerial LiDAR system consists of three main parts: a laser scanner device, a GNSS positioning system, and an inertial measurement unit (IMU) sensor (Vo et al., 2016; Pereira and Janssen, 1999; Habib et al., 2005; Hollaus et al., 2005). The post-processing of the distance between the scanner and the target and the position and attitude data obtained from GNSS and IMUs are used to determine the target's location in the 3D space (Dong and Chen, 2017; Pfeifer and Briese, 2007).

The coordinates of the target points, as seen in Fig. 1, are obtained by combining the measurements from all system's parameters. In this figure, $\vec{X}_G$ is the position vector of the ground point of the laser, which can be determined by summing-up three vectors $\left(\vec{X}_O, \vec{P}_G, \vec{\rho}\right)$ after applying the appropriate rotations $R_{y,p,r}$, $R_{\Delta\omega,\Delta\varphi,\Delta\kappa}$ and $R_{\alpha,\beta}$ at any time. $\vec{X}_O$ is the translation vector from the origin of the ground reference coordinate system to the origin of the GNSS/IMU body frame, $\vec{P}_G$ is the offset between the GNSS/IMU coordinate system and the laser unit (lever-arm offset vector) and $\vec{\rho}$ is the distance vector from the laser pulse firing point to its footprint (effective surface of the wave return) (Shan and Toth, 2018).

The process of determining the three-dimensional position of target objects, typically involves calculating the longitude, latitude, and geodetic elevation in the World Geodetic System 1984 (WGS-84). These coordinates can then be transformed into a local or national grid, and the geodetic heights can be converted to the orthometric system using a geoid model (Webster and Dias, 2006).

Since 2008, ALS systems have undergone significant advances, particularly in capturing multiple return signals for improved topographic mapping in dense vegetation (Pourali et al., 2014; Reutebuch et al., 2005; Sheng et al., 2003). Notable progress includes enhancements in pulse frequency, ranging accuracy, and signal intensity data availability (Toth, 2004). These improvements have led to higher-quality data, enabling aerial laser scanning applications to expand across various fields, such as mapping land surface topography, generating DEMs and DTMs (Maas, 2003; Webster et al., 2004; Renslow, 2013), forestry modeling and analysis (Hancock et al., 2012; Bazezew et al., 2018; Qi et al., 2023), airborne traffic monitoring (Yao et al., 2011), landslides and subsidence investigation (Pirasteh and Li, 2018), 3D building modeling (Aguilera et al., 2013), road extraction (Fernández-Arango et al., 2022), watershed analysis, flood risk assessment (Muhadi et al., 2020), and even snow depth measurement (Deems et al., 2013). The versatility of aerial LiDAR technology demonstrates its importance and value in modern applications.

1.2. Challenges, accuracy evaluation and error mitigation

The quality of the point cloud acquired from a LiDAR system is influenced by systematic errors, random noise in measurements, and various sensor parameters. Random errors arise from the accuracy of system measurements, encompassing positioning, alignment, scanner mirror angle, and measured length. Conversely, systematic errors are predominantly attributed to angular parameter biases (Hodgson et al., 2005). Overall, LiDAR system errors can be categorized into four main types. The first category comprises navigation system errors, encompassing GNSS and INS (Inertial Navigation System). GNSS errors include ionospheric and tropospheric errors, orbital errors, phase ambiguity, and satellite configuration geometry. INS errors involve gyroscope drift and errors in Roll, Pitch, and Yaw angles. The second category corresponds to scanner-related errors, including laser length measurement errors and scanner data recording errors. The third category pertains to the fusion of GNSS, INS, and laser scanner systems, involving transformation errors between sensors and their coordinate systems, as well as synchronization errors among data. The fourth category entails environmental errors, encompassing atmospheric conditions, land geometry, and land cover types (Liu, 2011). By understanding and mitigating these different types of errors, the overall accuracy and reliability of LiDAR point cloud data can be improved.

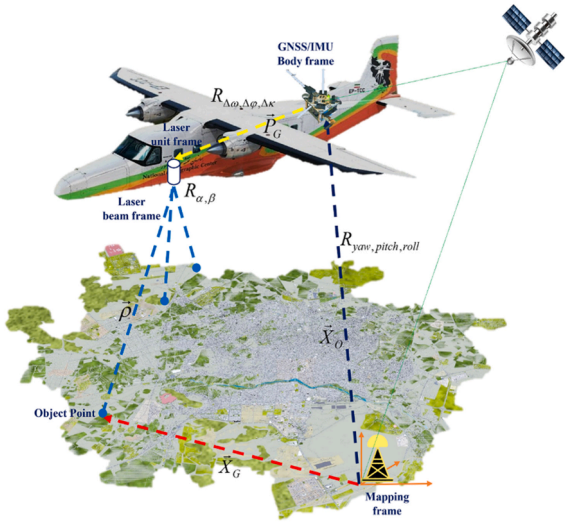

Fig. 1. Coordinate systems and LiDAR measurement parameters.

Calibration is crucial for achieving the highest accuracy in ALS systems. The calibration process involves pre-flight calibration by the manufacturer and post-flight calibration to determine parameters that cannot be directly measured (Habib et al., 2010a). Quality assurance (QA) procedures are carried out before data collection to ensure desired data quality, while quality control (QC) procedures are conducted afterward to verify if the achieved data quality meets the required standards. External QC methods involve comparing LiDAR data with higher-accuracy height models using ground targets. However, external QC methods can be time-consuming and costly (Shan and Toth, 2018; Liu et al., 2007; Csanyi and Toth, 2007; Vosselman et al., 2001). The lack of a well-defined quality control process raises concerns about the quality of LIDAR-derived footprints. To address this, in 2010, Habib et al. proposes an approach for evaluating LiDAR data quality by assessing the coincidence of conjugate surface elements in overlapping strips (Habib et al., 2010b). The methodology involves manipulating range and intensity images, linear features extraction, and areal patches from overlapping strips, and introduces a surface matching procedure. Kersting et al. (2012) introduced an automated calibration technique that concentrates on identifying system parameters by reducing inconsistencies among corresponding surface elements in overlapping strips, along with utilizing control data if accessible. The approach employs strong matching methods and incorporates appropriate primitives without requiring data preprocessing. The experimental findings confirm the efficiency of this proposed calibration method across various types of terrain coverage (Kersting et al., 2012). To enhance the calibration process in the LiDAR community, it is crucial to develop universally accepted protocols. This improvement should focus on investigating essential parameters and error sources, while developing accurate methods to estimate them without causing correlation issues. Additionally, robust calibration procedures must be created to handle diverse LiDAR data scenarios, even when raw measurements and control information are limited. Identifying relevant features for recognition in overlapping strips and control surfaces, especially for different terrains, is essential. Mathematical constraints should be integrated to combine system parameters and recognized features seamlessly. Lastly, standardized procedures and metrics should be established to assess the accuracy and quality of estimated system parameters (Habib and Rens, 2007).

LiDAR data typically exhibit higher height accuracy compared to horizontal accuracy, although advancements have been made in improving the horizontal accuracy (Qiao et al., 2010; Wu et al., 2015; Hodgson et al., 2003). Determining the accuracy of LiDAR data's height measurements often involves comparing the obtained DEM with ground control points (GCPs). However, it is important to consider that the expansion of DEM elevations to cell-covered areas can introduce errors during the comparison process with GCP elevations (Maune et al., 2007). Alternatively, comparisons can be made by examining individual LiDAR points against GNSS benchmark points to validate the accuracy of point cloud. Additionally, by utilizing appropriate interpolation methods, GCP height values can be used to evaluate the height accuracy of surrounding LiDAR points. Evaluating the accuracy of LiDAR data requires an adequate number of well-distributed control points (Hodgson and Bresnahan, 2004).

It is worth noting that the accuracy of LiDAR can be influenced by the type of land cover present. For example, areas with dense vegetation may experience greater errors compared to open land areas (NDEP, 2004). It is also known that collecting a large number of points with high-precision coordinates gives a higher level of reliability, but it can be a time-consuming and expensive task (Maune et al., 2007). To estimate the height accuracy of the LiDAR data, the height of each control point is compared with the surrounding LiDAR points within a certain radius, and the height RMSE (Root Mean Squares Error) is calculated (Webster, 2005).

Recent studies emphasize the importance of improving the accuracy of LiDAR point clouds and DEM, particularly in the height component. Huising and Gomes (1998) stated that LiDAR data height accuracy may vary from 5 to 200 cm, as one of the earliest estimates (Huising and Pereira, 1998). Bowen and Waltermire (2002) evaluated LiDAR data from the Richland area of South California and found a horizontal accuracy of 120 cm (Bowen and Waltermire, 2002). Xhardé et al. (2006) analyzed data from a Canadian province and reported a horizontal accuracy of 54 cm and a height accuracy of 16.5 cm (Xhardé et al., 2006). Other studies have also indicated a range of 26–153 cm for height accuracy in large-scale LiDAR surveys (Hodgson et al., 2003; Adams and Chandler, 2002). Montane (2006) focused on LiDAR points in an Icelandic salt marsh and found an average elevation difference of 7 cm between RTK and ALS data (Montane and Torres, 2006).

There have also been attempts to enhance the accuracy of LiDAR data. Csanyi and Toth (2007) emphasized the use of GCPs to improve LiDAR accuracy, achieving accuracy within a few centimeters through target point integration (Csanyi and Toth, 2007). Habib (2008) reported a horizontal accuracy of 50 cm and height accuracy of 15 cm for a point cloud collected using the OPTECH ATLM 2070 airborne scanner at an altitude of 975 m (Habib, 2008). These studies provide insights into early estimates, variations in accuracy levels, the impact of specific environments, and methods to enhance accuracy through ground control points. Most LiDAR point cloud providers have claimed an elevation RMSE value of 15 cm in recent years, even though such accuracy can only be obtained in ideal conditions (Hodgson et al., 2003). As the largest manufacturer of aerial laser scanning systems, Optech claims an elevation accuracy of 15 cm for the ATLM system. This value is widely used by laser scanning service providers and data distribution centers (Maas, 2003).

1.3. Recent developments and research gap

In recent years, by incorporating various spatio-temporal elements, such as GNSS, raw inertial, image, and LiDAR data, the accuracy of attitude determination with compact inertial sensors has been greatly enhanced. This method benefits kinematic laser scanning on lightweight aerial devices like drones, leading to more accurate and self-consistent geo-referenced point clouds (Mouzakidou et al., 2024). Wallace et al. (2012) proposed an algorithm that combined GPS, IMU, and High-Definition video camera observations to demonstrate that incorporating video data improves the horizontal accuracy of the final point cloud RMSE, reducing it from 61 cm to 34 cm (Wallace et al., 2012). To integrate spectral and geometric information gathered by low-cost UAVs (Unmanned Aerial Vehicles), accurate registration of LiDAR point clouds and images is necessary. Li et al. (2019) introduced NRLI-UAV, a non-rigid registration method for sequential raw laser scans and images taken by low-cost UAV systems. The assessment of LiDAR point cloud quality

using plane fitting showed improvement from 45 cm to 5 cm (RMSE of plane fitting) when using NRLI-UAV, demonstrating high automation, robustness, and accuracy (Li et al., 2019). De Oliveira and Santos (2019) aimed to meticulously calibrate UAV-based LiDAR systems by refining boresight angles using a point-to-plane method. This method displayed improved positional accuracy compared to existing techniques when assessing the accuracy of the adjusted point cloud to point/planar features (De Oliveira and Santos, 2019).

Real-Time Kinematic (RTK) technology has also significantly improved the precision of height measurements in LiDAR data. However, while recent advancements show great potential for increasing LiDAR height accuracy, there is a noticeable lack of studies employing the higher precision provided by GNSS techniques to combine it with LiDAR data, particularly in urban environments. Hladik and Alber (2012) conducted a study focusing on this area. They introduced a method that incorporated high-precision RTK observations to improve the accuracy of a digital elevation model for a salt marsh. Their approach successfully reduced the RMSE from 16 cm to 10 cm (Hladik and Alber, 2012). Schmelz and Psuty (2019) conducted another study to evaluate the reliability of LiDAR data in detecting coastal geomorphological changes. They achieved a reduction in the height RMSE of the LiDAR data from 50 cm to 25 cm by systematically adjusting the offsets between the LiDAR data and the ground truth (Schmelz and Psuty, 2019). Elaksher et al. (2023) conducted an extensive assessment of a LiDAR system, aiming to measure the accuracy and quality of its data. Their findings revealed an average elevation discrepancy of 12 cm when comparing the LiDAR data to the results obtained from terrestrial surveying. Additionally, the horizontal offsets exhibited an RMSE of approximately 50 cm (Elaksher et al., 2023).

1.4. Proposed research

The approach we propose has the high potential to address the above-mentioned scarcity of substantial research and contribute to the broader adoption of this technique across various remote sensing scenarios. We aim to address this research gap by employing a more efficient and cost-effective method to improve the accuracy of DEMs, specifically in urban areas. Our focus is on investigating the accuracy enhancement of LiDAR point cloud coordinates. To achieve this, we propose a novel method that utilizes the fusion of ultrasonic devices and NRTK data to retrieve ground-level heights.

In the course of this study, we developed and utilized a prototype, implementing a suitable and comprehensive model to enhance the accuracy of LiDAR point height coordinates. The effectiveness of our method was further validated through independent checkpoints. Our study introduces a methodology for rapidly and accurately enhancing the height component accuracy of LiDAR point clouds in urban environments. In addition, it highlights the high potential of integrating ultrasonic devices and NRTK data. By enhancing the accuracy of LiDAR point cloud data, the proposed method provides promising results to improve the accuracy of DEM models and therefore enhancing 3D urban mapping.

2. Materials and methods

A cost-effective prototype is specifically designed and deployed for acquiring ground data to improve the accuracy of LiDAR height measurements. The core principle of this approach entails using a substantial amount of ground-level converted RTK-GNSS data to address systematic errors inherent in the LiDAR point cloud. These errors may stem from inaccuracies in the positioning system or the attitude parameters of the ALS device (Vosselman and Maas, 2010). Given that LiDAR points are acquired along a flight line these systematic errors may be associated either with the flight path or the date of observations.

In contrast to previous research that relied on GCPs to investigate LiDAR data accuracy, this study takes a different approach. It utilizes a significantly large number of ground target points to enhance the accuracy of LiDAR point cloud heights, without any prior information about individual LiDAR cloud points. The approach involves the utilization of a correction surface that incorporates the spatio-temporal variations of height errors. This correction surface is generated by calculating the differences between LiDAR heights and Network-Real-Time Kinematic measurements. Due to the limited availability of GCP points, an NRTK–Ultrasonic platform is developed to augment the number of reference points.

The methodology employed in this research is briefly illustrated in Fig. 2 and presented in detail in the subsequent section.

2.1. NRTK-ultrasonic prototype development

To automatically determine ground-level heights using NRTK, the approach involve installing a GNSS receiver on the vehicle's rooftop. However, it was crucial to accurately measure the vertical position of the GNSS platform relative to the road surface at all time instances. This was challenging due to potential variations in the vehicle's height caused by the suspension system. To overcome this, ultrasonic sensors were employed to measure the distance between the car body and the road, with a minimum of two sensors, placed on each side of the vehicle (Fig. 3-a). Considering the data collection in urban environments with dense vegetation and tall buildings, using multiple GNSS receivers was preferred to reduce the risk of losing NRTK coordinates. This was observed during implementation, where one or two out of the three devices used often failed to establish fixed coordinates.

Based on Fig. 3-b, the subsequent action involves incorporating the predetermined distance between the car's roof platform and the altimeter sensor located on both sides of the vehicle. This allows for the determination of the height of the platform surface relative to the ground level. Additionally, during this stage, the height measured by the NRTK receivers is shifted to the platform by considering the GNSS antenna height.

2.2. Study area and data acquisition

The Austrian RIEGL LMS-Q560 laser scanner was used to collect the LiDAR data for this study. A Dornier aircraft conducted a flight at a height of approximately 800 m above the ground, traveling at a speed of 216 km/h. The laser scanner had a return pulse

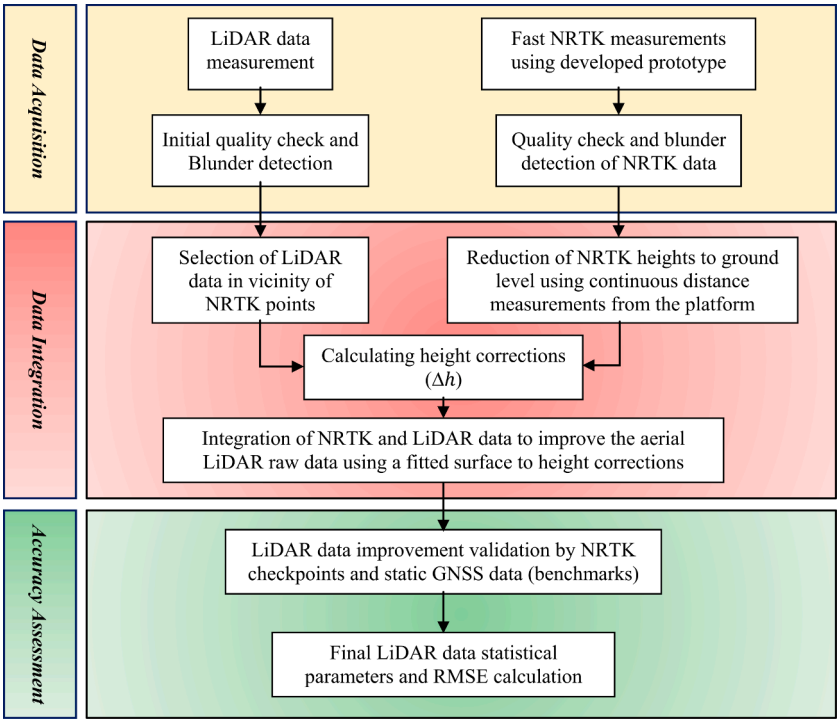

Fig. 2. LiDAR height accuracy improvement methodology.

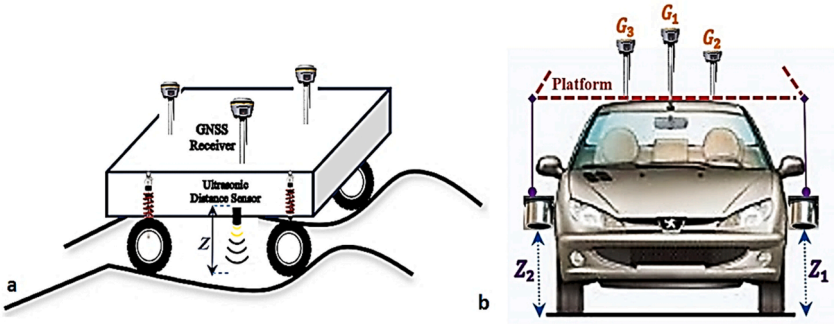

Fig. 3. a) NRTK and ultrasonic fusion for precise height measurements concept, b) Data collection and geometry of vehicle-mounted surveying instruments (Z_1 and Z_2 are the ultrasonic distance measurements).

frequency of 120 kHz and a scan angle of 60°. In total, the city of Isfahan yielded around 900 million elevation points, with an estimated density of 2.8 points per square meter and an average distance of 50 cm between each point. These points were obtained through 38 flight lines. Fig. 4 illustrates an example of the collected LiDAR data symbolically.

To carry out the field measurements of the research, as there is land subsidence in the northern part of the city, we have selected an area with practically no subsidence and the GNSS-NRTK measurement was performed for about 173 million LiDAR points in the south part of the area (Fig. 5).

On January 10, 2020, data was simultaneously collected in this area for NRTK-ultrasonic distance measurement. The collection took place from 9:00 a.m. to 7:00 p.m. A total of 135 km of roads were covered, with an average speed of 30 km/h. For field sampling, three 220-channel multi-frequency SOUTH Galaxy-G1 receivers were used, with a nominal measurement accuracy of 8 mm + 0.5 ppm for horizontal coordinates and 15 mm + 0.5 ppm for height coordinates. Additionally, two HC-SR04 ultrasonic distance measuring sensors were installed on the Peugeot-206 Sedan, with a nominal accuracy of 3 mm for distance measurements between 2 cm and 400 cm. Three GNSS receivers were mounted on the vehicle's roof platform. Two distance measurement sensors were also placed on each side of the vehicle to measure changes in height relative to the ground surface (Fig. 6). The antenna height of each GNSS receiver, the constant height of each distance sensor relative to the platform surface, and the height of the platform on both sides from the ground surface were all measured for later calculations.

The national NRTK system, provided by Leica Geosystems, was used to measure GNSS coordinates. Simultaneous ultrasonic ranging was conducted to align the NRTK points with the ground level. The measurement and storage rates were set at 1 s. Table 1 dis-

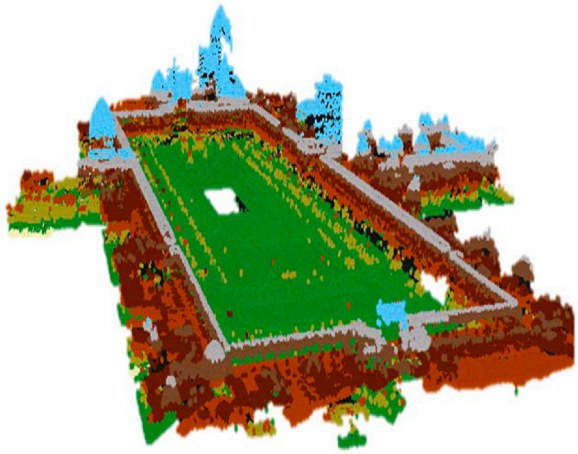

Fig. 4. An example of LiDAR data collected in the city of Isfahan (related to Naqsh-e Jahan historical square).

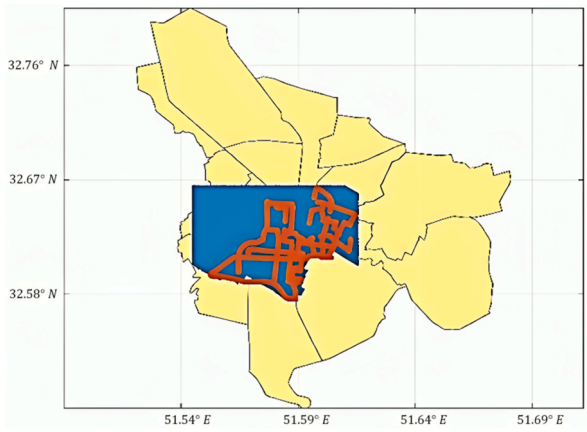

Fig. 5. NRTK and ultrasonic ground data survey routes (Orange color), LiDAR data area (Blue). Isfahan City districts (Yellow). (For interpretation of the references to color in this figure legend, the reader is referred to the Web version of this article.)

Fig. 6. The Prototype configuration: a) GNSS receivers installed on the platform, b) HC-SR04 ultrasonic distance Measuring Module 33 V/5V devices on vehicle's both sides.

plays the volume of data that were collected. Synchronization of GNSS and ultrasonic sensor data was conducted, and the processing was accomplished using MATLAB software.

2.3. Accuracy enhancement for height estimation

To validate the accuracy of the fixed NRTK measurements, the lengths of the baselines formed between any pair of antennas on the platform surface were estimated using the NRTK results. By comparing these estimated lengths with the known lengths of the baselines, any outliers in the NRTK data were identified and removed. Two different methods were employed to calculate the height of the

Table 1
Number of stored ranging and positioning data.

Instrument Type	No. of data
Ultrasonic Sensor-Left side	17522
Ultrasonic Sensor-Right side	17522
SOUTH Galaxy GNSS NRTK (G_1)	14455
SOUTH Galaxy GNSS NRTK (G_2)	13142
SOUTH Galaxy GNSS NRTK (G_3)	11303

center point of the platform using the available GNSS receiver data. In the first method, where all three NRTK data were available, the centroid of the triangle formed by the GNSS positions on the platform was estimated using a coordinate averaging approach. The height of the centroid was then determined by combining the altimeter data and the Inverse Distance Weighting (IDW) method. The IDW method utilized an interpolation technique to estimate the precise height between the platform and the actual ground surface. It involved calculating the height of the unknown point $\boldsymbol{C}$ based on the inverse ratio of the distances between the GNSS points with known using the following equation:

$$Z_C = l + \frac{\sum_{i=1}^{2}\left(\frac{z_i}{d_i}\right)}{\sum_{i=1}^{2}\left(\frac{1}{d_i}\right)} \tag{1}$$

where $\boldsymbol{Z_C}$ is the distance between the ground and the centroid, $\boldsymbol{l}$ is the constant distance from the leveled platform to the ultrasonic sensor, $\boldsymbol{d_i}$ is the horizontal distance of each sensor to the centroid, and $\boldsymbol{z_i}$ is the range measurement of each distance sensor (Fig. 7).

Due to the obstacles and buildings in urban areas, we may face signal interruption for one or two GNSS devices. When missing one receiver, the center of gravity on the connecting line between the other two receivers is used to calculate the height of point $\boldsymbol{C}$. In the case where only one receiver's data was available, the position of this receiver is used as point $\boldsymbol{C}$, while this case has rarely occurred.

2.4. LiDAR height error estimation

After calculating the height of the centroid point $\boldsymbol{C}$ using one of the methods mentioned above, the geodetic height of the corresponding target point ($\boldsymbol{P_i}$) on the ground surface (i.e., in the roadway) is calculated using the following equation:

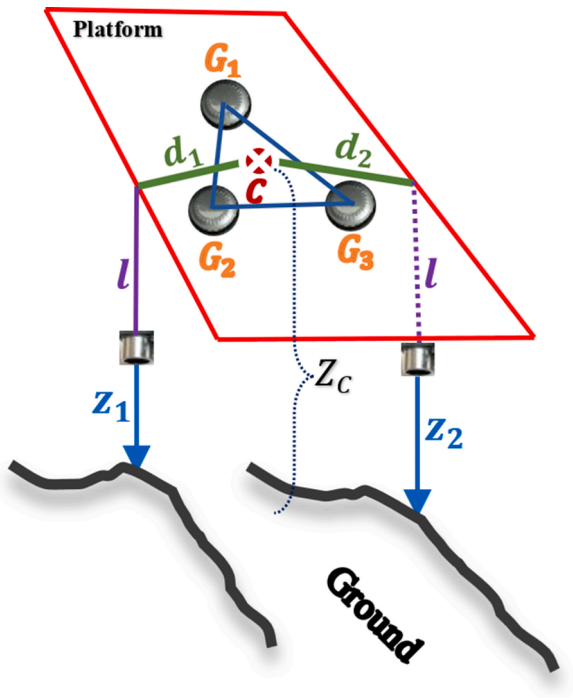

Fig. 7. Calculating centroid (C) height using all GNSS observations and ranging data.

$$h_{Pi(NRTK)} = h_C - Z_C \tag{2}$$

where h_C is the geodetic height of point C on the platform and Z_C is the distance from the centroid to ground C.

The LiDAR points were clipped and refined in the next step based on the NRTK surveyed area. For each NRTK point as a target point (P_i), considering the density of LiDAR points, 10 points were selected (which corresponds to about 3.5 m^2 of surface that seems appropriate for this experiment given the surface of the car roof) from the surrounding LiDAR points (Fig. 8). The LiDAR points' 3D distance from the target point is calculated. If the mean of these distances exceeds 2 m, the LiDAR points and the target point are removed from the further computation process. The reason for choosing a sphere radius smaller than 2 m is to avoid selecting points with inconsistent height differences in a neighborhood, especially on roads with different levels. In determining the neighborhood radius, in addition to the 2-m distance, a 1-m radius was also considered. The choice of this radius depends on the average width of the roads and the dimension of the car.

The NRTK target point's elevation was subsequently determined by applying the IDW technique to ten adjacent LiDAR points. In this calculation, a parameter of two was employed to achieve a smoother surface (Eq. (3)):

$$h_{Pi(Lidar)} = \frac{\sum_{j=1}^{10} \left(\frac{h_{j\,(Lidar)}}{d_j^2(Lidar)} \right)}{\sum_{j=1}^{10} \left(\frac{1}{d_j^2(Lidar)} \right)} \tag{3}$$

where $h_j(Lidar)$ is the height of each LiDAR point around P_i and d_j is the distance between the LiDAR point and P_i.

In the next step, the difference between the height of the NRTK target points obtained from LiDAR, and the height of the NRTK-ultrasonic point, was calculated (Eq. (4)):

$$\Delta h_{Pi} = h_{Pi(Lidar)} - h_{Pi(NRTK)} \tag{4}$$

2.5. LiDAR heights correction surface

The height differences between LiDAR and NRTK along the roads within the study area are used to generate a correction surface, as shown in Fig. 10. This correction surface can be employed to enhance the LiDAR height values of other points. One practical approach is to utilize spatial interpolation methods. In this study, the natural neighbor interpolation method was implemented. This method relies on the Voronoi tessellation of a discrete set of spatial points. The fundamental Equation for this method is:

$$\Delta h_L = \sum_{i=1}^{n} W_i(L)\, \Delta h_{Pi} \tag{5}$$

where Δh_L is the estimate of the LiDAR height correction at a LiDAR point L, the weights W_i are calculated by finding the stolen areas, after inserting the calculation point L in the Voronoi tessellation from the surrounding areas (Fig. 9). The Sibson's weights are used, which could be calculated as follows:

$$W_i(L) = \frac{\mathscr{A}(P_i)}{\mathscr{A}(L)} \tag{6}$$

where $\mathscr{A}(P_i)$ are the stolen areas of surrounding Voronoi polygons from $\mathscr{A}(L)$, which is the area around point L after inserting this point in the Voronoi tessellation (Dong and Chen, 2017; Sibson and Barnett, 1981).

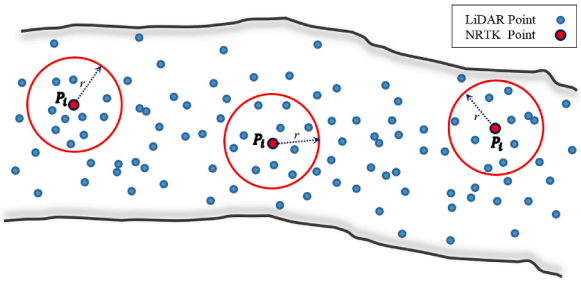

Fig. 8. Selection of LiDAR points around each NRTK ground target point along the vehicle's path.

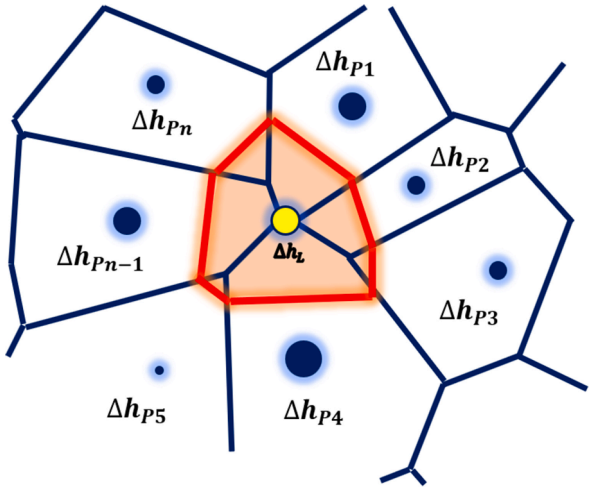

Fig. 9. Natural neighbor interpolation.

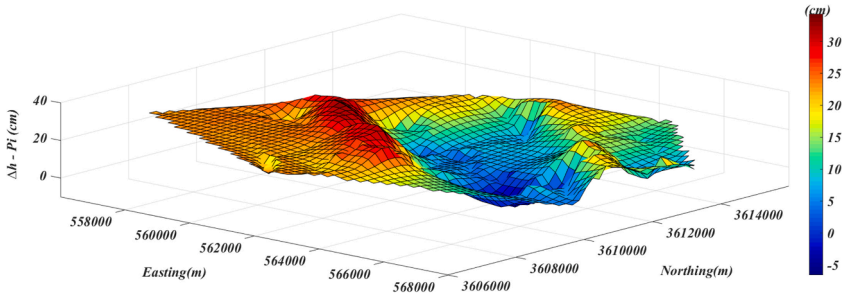

Fig. 10. Height correction surface of the current study.

2.6. Assessing the improvement of LiDAR data

At this stage, GNSS points are measured across the surveyed area and used for benchmarking purposes. Both static and NRTK methods are employed to obtain accurate height measurements. To compare the accuracy of LiDAR height values, the IDW method is utilized. The LiDAR height and LiDAR height correction values at the benchmark points are estimated using the IDW method. So, ten surrounding LiDAR points, whose height correction value was calculated from the surface of Fig. 10 and according to Equation (4), were used. These points were selected in a radius with a maximum radial distance of 1 or 2 m so that the estimation of height correction of these benchmarks can be calculated according to Fig. 11 and Equation (7).

$$\Delta h_{BM} = \frac{\sum_{i=1}^{10}\left(\frac{\Delta h_{Li}}{d_i^2}\right)}{\sum_{i=1}^{10}\left(\frac{1}{d_i^2}\right)} \tag{7}$$

In the same way, the LiDAR height in the benchmark location is estimated using the IDW method (h_{BML}). Finally, the height difference value of each GNSS control point from the ellipsoid surface and its estimated height, Δh_{Total} will be determined as follows.

$$\Delta h_{Total} = \left[h_{BML} - \Delta h_{BM}\right] - h_{BM} \tag{8}$$

3. Results and discussion

3.1. Comparing the NRTK target points and LiDAR heights

From Eq. (4), the difference between the height of the target points estimated from the LiDAR points and the height calculated by NRTK measurements (after applying the measurement of the ultrasound sensor) was calculated. For this purpose, according to Fig. 8, different radial distances were used to calculate the value of Δh_{Pi} so that for each ground target point, 10 neighboring LiDAR points were selected at the closest distance from that point. The value of statistical parameters for height difference was calculated. The results are shown in Table 2.

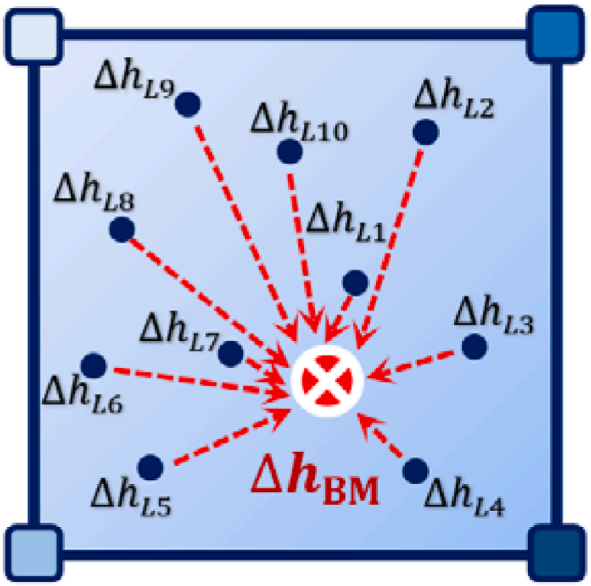

Fig. 11. LiDAR Height correction at benchmark location using IDW method from nearby LiDAR points.

Table 2
The estimated height accuracy of LiDAR raw data using ground target points.

Radial distance (m)	No. of NRTK -Target pts	Mean (cm)	STD (cm)	MAE (cm)	RMSE (cm)
2	11219	18.2	13.2	20.6	25.0
1	5503	13.6	9.0	14.8	17.3

As can be seen in Tables 2 and if the LiDAR points are selected around each ground target point up to a maximum radial distance of 2 m, it is possible to choose 11,219 ground target points, with a mean difference of 18.2 cm, a standard deviation of 13.2 cm, the MAE value of 20.6 cm, and the RMSE value of 25 cm for $\Delta \boldsymbol{h_{Pi}}$. When the neighborhood radius is less than 1 m, the mean difference is 13.6 cm, the standard deviation is 9.0 cm, the MAE is 14.8 cm, and the RMSE is 17.3 cm. With this radius, only 5503 ground target points have remained.

Fig. 12 illustrates the distribution of the final $\Delta \boldsymbol{h_{Pi}}$ values along the roads within the study area. A clear systematic behavior can be observed in the distribution of LiDAR height errors. These errors are likely associated with positioning or attitude errors along the flight path or the date of observations. Furthermore, for this research, it is not essential to consider the relationship between the errors and the flight path or the timing of LiDAR measurements. The presence of a pattern in the LiDAR height error is adequate to apply our approach. Our attempt to minimize these errors was through automated NRTK measurements, as explained earlier. This spatial behavior may be influenced by various environmental and measurement conditions, such as the accuracy of flight path restitution, sloping terrain, multipath reflection, and GNSS/IMU calibration, among others (Vosselman and Maas, 2010).

To correct the height of the LiDAR points (or estimate the amount of correction at any desired point), a surface was fitted to the values of the $\Delta \boldsymbol{h_{Pi}}$ According to Fig. 10.

3.2. Verification of LiDAR height correction using GNSS benchmarks

To evaluate the effectiveness of the proposed algorithm, benchmark points situated along the roads of Isfahan city were employed. The precise coordinates of these benchmarks were obtained using the static GNSS positioning method. Initially, the benchmarks were chosen within the correction surface region (Fig. 13).

In the subsequent step, 10 neighboring LiDAR points were chosen around each benchmark point, with radial distances of either 2 m or 1 m. The benchmark heights were then derived from the raw LiDAR data using the IDW method, where the reciprocal square of the distance was used as the weight. This process was performed twice, once for a 2-m radius and again for a 1-m radius.

When considering a 2-m radius, 72 benchmark points had a minimum of 10 LiDAR points in their vicinity. In this case, the height RMSE was 21.2 cm. Alternatively, when considering a maximum radius of 1 m around the benchmark points, the number of benchmark points was reduced to 45, and the RMSE was reduced to 18.5 cm. The differences between the corrected LiDAR heights (using the proposed correction surface) and the benchmark points were calculated using equations (7) and (8). As expected, upon correcting the heights using a radial distance of 2 m, the RMSE decreased to 8.8 cm for the 72 points. Further reducing the maximum radial distance to 1 m resulted in an improved RMSE of 8.2 cm. More detailed results can be found in Table 3.

Fig. 14 illustrates the $\Delta \boldsymbol{h}_{\boldsymbol{Total}}$ for 45 BMs before and after applying the height correction to calculate the BM heights from the LiDAR points considering a maximum radius of 1 m for the BMs neighborhood.

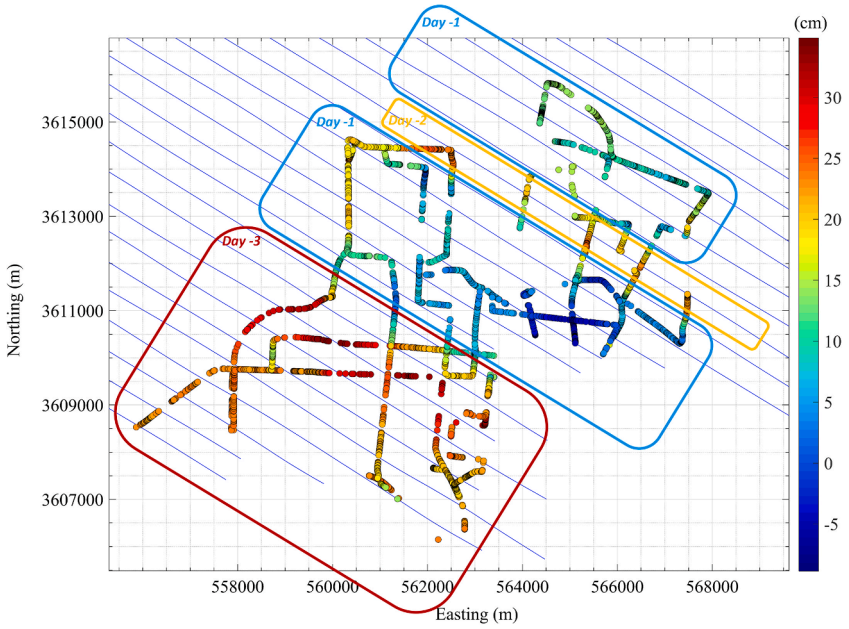

Fig. 12. LiDAR height error (Δh_{Pi}) values distribution along the surveyed routes (scatter dots), flight paths (thin oblique blue parallel lines), and the observations day (rectangles). (For interpretation of the references to color in this figure legend, the reader is referred to the Web version of this article.)

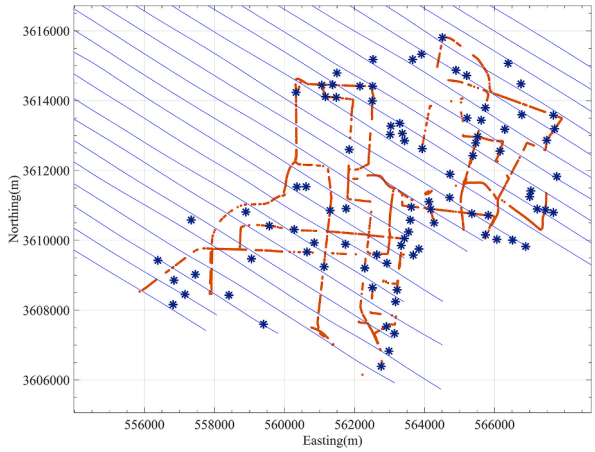

Fig. 13. Distribution of GNSS benchmarks (navy blue star points), NRTK survey path (Orange color line), and flight path (thin blue lines) in the study area. (For interpretation of the references to color in this figure legend, the reader is referred to the Web version of this article.)

Table 3
Estimated height accuracy of LiDAR data using GNSS control points.

Error Estimation phase	Radial distance (m)	No. of Control points	Mean (cm)	STD (cm)	MAE (cm)	RMSE (cm)
Before Correction	2	72	17.3	12.4	17.6	21.2
	1	45	14.9	11.1	15.2	18.5
After Correction	2	72	1.5	8.7	6.9	8.8
	1	45	0.1	8.3	6.9	8.2

According to the data presented in Table 3, implementing the corrections with a neighborhood radius of 1 m resulted in a significant decrease of 55.7% in the RMSE. Moreover, the standard deviation, mean and mean absolute error (MAE) values have shown substantial improvement.

3.3. Verification of LiDAR height correction using NRTK points

To further assess the effectiveness of the correction surface, the observed NRTK target points were utilized. Out of approximately 5500 NRTK points, a random selection of around 1000 points was designated as checkpoints. The remaining 4500 points were used to create the correction surface. The height of the checkpoints was estimated using both the raw and corrected LiDAR points and then compared with the reduced NRTK height values that represent the road surface.

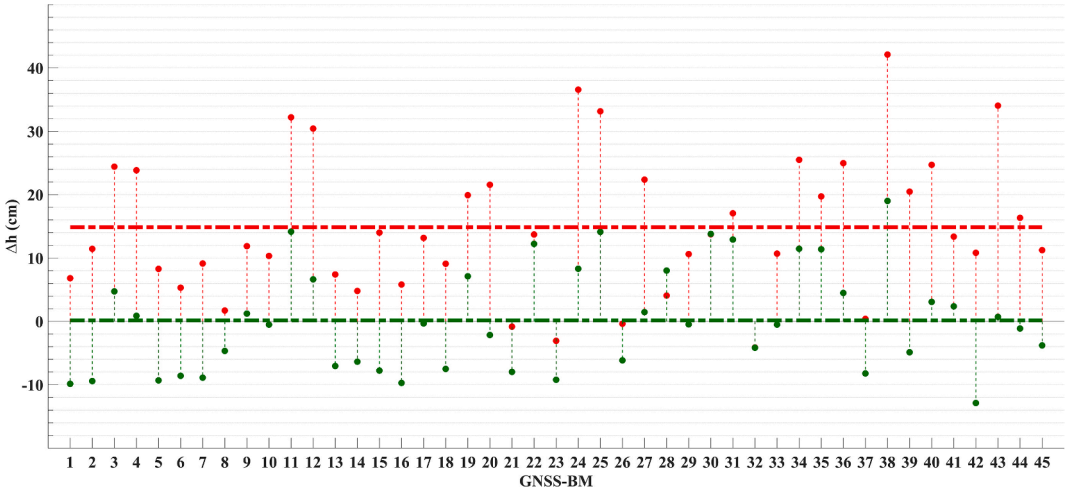

Fig. 14. Δh_{Total} values for GNSS BMs (before implementing the correction surface: red-dotted stem, after correction with the surface: green-dotted stem, mean error before correction: red long-dashed line and mean after correction: green long-dashed line). (For interpretation of the references to color in this figure legend, the reader is referred to the Web version of this article.)

The application of the proposed correction resulted in significant improvements in the heights of the LiDAR points, as demonstrated in Table 4. The height RSME of the LiDAR data decreased by 69.5% after the corrections were applied. The reduction in other statistical parameters is also evident from the data presented in Table 4.

Fig. 15 illustrates the changes in LiDAR height errors across 958 target points, showing an improvement in the average height error following the application of the corrections.

We have also examined the density of NRTK points in relation to the effectiveness of the correction surfaces. The quantity of NRTK points was gradually reduced in multiple stages to evaluate the improvement of LiDAR data. In order to accomplish this, we utilized 500, 1000, and 4500 NRTK points to construct the correction surface, and then estimated the statistical parameters of the corrected LiDAR data using 953 check-points. As indicated in Table 5, when there is a satisfactory number of LiDAR points surrounding the ground NRTK points, the proposed algorithm significantly enhances the accuracy of the LiDAR data.

Table 4
Correction surface efficiency check for LiDAR data using NRTK checkpoints.

Correction phase	Radial distance (m)	No. of Control points	Mean (cm)	STD (cm)	MAE (cm)	RMSE (cm)
Before	1	958	13.5	10.9	14.8	17.4
After	1	958	0.1	5.3	3.8	5.3

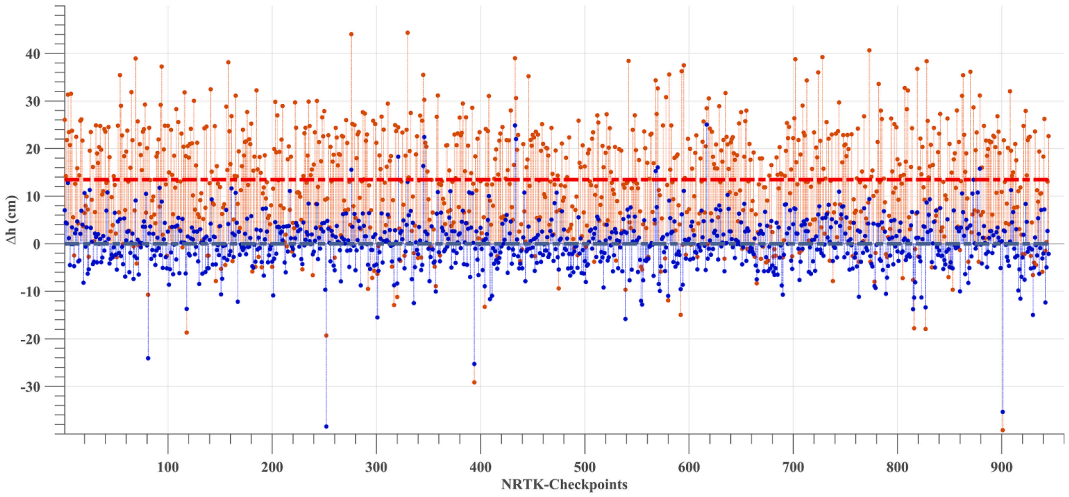

Fig. 15. Δh_{Total} values for NRTK checkpoints. (Before implementing the correction surface: red-dotted stem, after correction with the correction surface: blue-dotted stem, mean before correction: red long-dashed line and mean after correction: blue long-dashed line). (For interpretation of the references to color in this figure legend, the reader is referred to the Web version of this article.)

Table 5
The effect of the NRTK ground points density on the efficiency of the LiDAR data correction (verification over 958 check-points).

No. of ground NRTK -Target pts	Mean (cm)	STD (cm)	MAE (cm)	RMSE (cm)
500	−0.4	5.52	3.99	5.65
1000	−0.2	5.4	3.9	5.4
4500	0.1	5.3	3.8	5.3

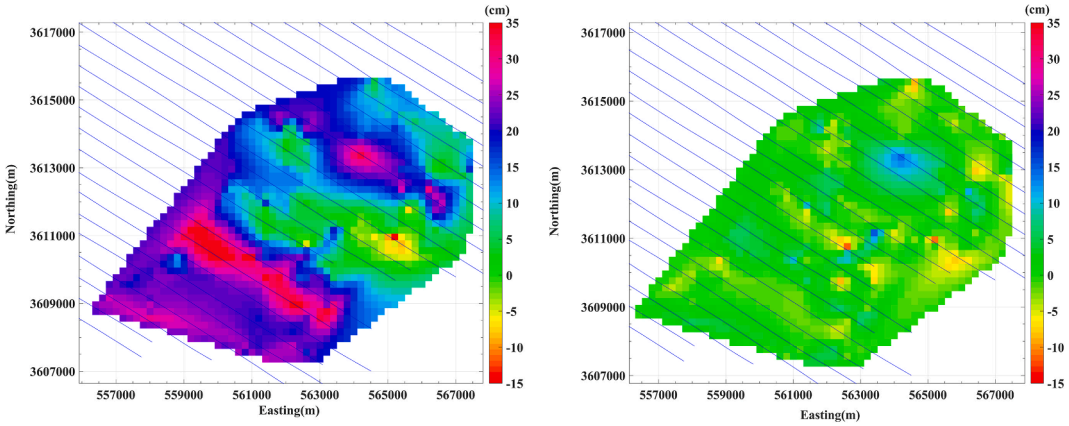

Fig. 16. RMSE over 1000 checkpoints' height before improvement (left plot), a quasi-homogeneous pattern of RMSE over the same points after the application of the correction surface (right plot).

Furthermore, an examination of the distribution of height errors in the study area was conducted before and after the application of the correction. Fig. 16 illustrates the height error pattern before employing the correction surface, which displays a noticeable correlation with the flight path and observation date. However, after the correction, this pattern is nearly eliminated, and the height errors of the LiDAR points are substantially reduced. As a result, the height errors over the NRTK checkpoints become more uniformly distributed across the study area.

4. Conclusions

This research focuses on enhancing the height accuracy of raw LiDAR data and explores the potential of high-density NRTK data to improve airborne LiDAR data. To achieve cost-effective and efficient data collection, a mobile ground data collection prototype was specifically constructed for observing road surface height. The prototype is developed with the concept of combining GNSS and distance measurements to quickly obtain ground level heights. The quality control assessment involved the utilization of static GNSS benchmarks and NRTK checkpoints. The results showed that the RMSE for height in the raw LiDAR data was 17.3 cm, with a mean error of 13.6 cm when using a 1-m neighborhood radius for selecting corresponding LiDAR points. To enhance the height accuracy of the LiDAR point cloud, a correction surface is introduced by utilizing automated NRTK positioning and distance measurements for road height estimation. This correction surface enables the improvement of height accuracy for any desired point within the LiDAR dataset. The results indicate a significant enhancement in the height accuracy of the LiDAR data when compared to the height of GNSS reference points. Upon the application of the correction surface, the average error was reduced to 0.1 cm, and the RMSE decreased to 8.2 cm. Moreover, incorporating around 1000 NRTK checkpoints and implementing the correction surface led to a significant reduction in the RMSE for the height of the LiDAR points. The RMSE decreased from 17.4 cm to 5.3 cm. Similarly, the mean error showed a notable improvement, decreasing from 13.5 cm to 0.1 cm. These substantial improvements confirm the effectiveness of the proposed method. Furthermore, by implementing the corrections to the LiDAR point elevations, the height error over checkpoints becomes nearly uniform throughout the entire study area. The systematic errors previously observed along paths almost parallel to the aircraft flight lines or associated with LiDAR observation date are effectively eliminated after improvement of the LiDAR heights. Further research should investigate the efficacy of the proposed method in enhancing LiDAR accuracy for non-ground classes, including building rooftops. Moreover, the platform employed in this project, which integrates distance measurement and NTRK, exhibits potential for various applications such as determining road height and slope, calculating the International Roughness Index (IRI) for roads, and measuring land subsidence.

Ethics

In the preparation of this article, the principles of research ethics were fully respected. All authors have approved the manuscript and agree with its submission to the Remote Sensing Applications: Society and Environment. We confirm that this manuscript is original, has not been published elsewhere, and is not currently under review by any other journal.

CRediT authorship contribution statement

Milad Salehi-Dorcheabedi: Writing – original draft, Visualization, Software, Methodology, Investigation. **Jamal Asgari:** Writing – review & editing, Validation, Supervision, Methodology, Conceptualization. **Alireza Amiri-Simkooei:** Writing – review & editing, Validation, Methodology. **Sayyed Bagher Fatemi Nasrabadi:** Writing – review & editing, Validation, Methodology.

Declaration of competing interest

The authors declare that they have no known competing financial interests or personal relationships that could have appeared to influence the work reported in this paper.

Data availability

Data will be made available on request.

Acknowledgments:

The authors would like to express their sincere gratitude to Isfahan Municipality for generously providing the LiDAR and GNSS benchmarks data used in this study.

References

Adams, J.C., Chandler, J.H., 2002. Evaluation of lidar and medium scale Photogrammetry for detecting soft-cliff coastal change. Photogramm. Rec. 17 (99), 405–418. https://doi.org/10.1111/0031-868x.00195.

Aguilera, D.G., Crespo-Matellan, E., Hernández-López, D., Rodríguez-Gonzálvez, P., 2013. Automated urban analysis based on LIDAR-derived building models. IEEE Trans. Geosci. Rem. Sens. 51 (3), 1844–1851. https://doi.org/10.1109/tgrs.2012.2205931.

Bazezew, M.N., Hussin, Y.A., Kloosterman, E.H., 2018. Integrating airborne LiDAR and terrestrial laser scanner forest parameters for accurate above-ground biomass/carbon estimation in ayer hitam tropical forest, Malaysia. Int. J. Appl. Earth Obs. Geoinf. 73, 638–652. https://doi.org/10.1016/j.jag.2018.07.026.

Bowen, Z.H., Waltermire, R.G., 2002. Evaluation of Light Detection and Ranging (LIDAR) for measuring river corridor topography. J. Am. Water Resour. Assoc. 38 (1), 33–41. https://doi.org/10.1111/j.1752-1688.2002.tb01532.x.

Csanyi, N., Toth, C.K., 2007. Improvement of LIDAR data accuracy using LIDAR-specific ground targets. Photogramm. Eng. Rem. Sens. 73 (4), 385–396. https://doi.org/10.14358/pers.73.4.385.

De Oliveira, E.M., Santos, D.R.D., 2019. Rigorous calibration of UAV-based LiDAR systems with refinement of the boresight angles using a point-to-plane approach. Sensors 19 (23), 5224.

Deems, J.S., Painter, T.H., Finnegan, D.C., 2013. Lidar measurement of snow depth: a review. J. Glaciol. 59 (215), 467–479. https://doi.org/10.3189/2013jog12j154.

Dong, P., Chen, Q., 2017. LiDAR remote sensing and applications. https://doi.org/10.4324/9781351233354.

Elaksher, A., Ali, T., Alharthy, A., 2023. A quantitative assessment of LIDAR data accuracy. Rem. Sens. 15, 442. https://doi.org/10.3390/rs15020442.

Favorskaya, M.N., Jain, L.C., 2017. Handbook on advances in remote sensing and geographic information systems. https://doi.org/10.1007/978-3-319-52308-8.

Fernández-Arango, D., Varela-García, F.-A., González-Aguilera, D., Lagüela-López, S., 2022. Automatic generation of urban road 3D models for pedestrian studies from LiDAR data. Rem. Sens. 14, 1102. https://doi.org/10.3390/rs14051102.

Habib, A., 2008. Accuracy, Quality Assurance, and Quality Control of LiDAR Data. CRC Press eBooks, pp. 269–294. https://doi.org/10.1201/9781420051438.ch9.

Habib, A., Rens, J., 2007. Quality Assurance and Quality Control of Lidar Systems and Derived Data, 10. InAdvanced lidar workshop, university of northern iowa, 9781420051438.

Habib, A., Ghanma, M., Morgan, M., Al-Ruzouq, R., 2005. Photogrammetric and LIDAR data registration using linear features. Photogramm. Eng. Rem. Sens. 71 (6), 699–707. https://doi.org/10.14358/pers.71.6.699.

Habib, A., Kersting, A.P., Bang, K.I., Lee, D.C., 2010a. Alternative methodologies for the internal quality control of parallel LiDAR strips. IEEE Trans. Geosci. Rem. Sens. 48 (1), 221–236. https://doi.org/10.1109/TGRS.2009.2026424. 5238545.

Habib, A., Bang, K.-I., Kersting, A.P., Chow, J.C.K., 2010b. Alternative methodologies for LiDAR system calibration. Rem. Sens. 2 (3), 874–907. https://doi.org/10.3390/rs2030874.

Hancock, S., Lewis, P., Foster, M.J., Disney, M., Müller, J.-P., 2012. Measuring forests with dual wavelength lidar: a simulation study over topography. Agric. For. Meteorol. 161, 123–133. https://doi.org/10.1016/j.agrformet.2012.03.014.

Hladik, C.M., Alber, M., 2012. Accuracy assessment and correction of a LIDAR-derived salt marsh digital elevation model. Rem. Sens. Environ. 121, 224–235. https://doi.org/10.1016/j.rse.2012.01.018.

Hodgson, M.E., Bresnahan, P., 2004. Accuracy of airborne LIDAR-derived elevation. Photogramm. Eng. Rem. Sens. 70 (3), 331–339. https://doi.org/10.14358/pers.70.3.331.

Hodgson, M.E., Jensen, J.R., Schmidt, L., Schill, S.R., Davis, B.A., 2003. An evaluation of LIDAR and IFSAR-derived digital elevation models in leaf-on conditions with USGS level 1 and level 2 DEMs. Rem. Sens. Environ. 84 (2), 295–308. https://doi.org/10.1016/s0034-4257(02)00114-1.

Hodgson, M.E., Jensen, J.R., Raber, G.T., Tullis, J.A., Davis, B.A., Thompson, G.S., Schuckman, K., 2005. An evaluation of LIDAR-derived elevation and terrain slope in leaf-off conditions. Photogramm. Eng. Rem. Sens. 71 (7), 817–823. https://doi.org/10.14358/pers.71.7.817.

Hollaus, M., Wagner, W., Kpayc, K., 2005. Airborne laser scanning and usefulness for hydrological models. Adv. Geosci. 5, 57–63. https://doi.org/10.5194/adgeo-5-57-2005.

Huising, E.J., Pereira, L.G., 1998. Errors and accuracy estimates of laser data acquired by various laser scanning systems for topographic applications. ISPRS J. Photogrammetry Remote Sens. 53 (5), 245–261. https://doi.org/10.1016/s0924-2716(98)00013-6.

Kersting, A.P., Habib, A., Bang, K.-I., et al., 2012. Automated approach for rigorous light detection and ranging system calibration without preprocessing and strict terrain coverage requirements. Opt. Eng. 51 (7), 076201.

Li, J., Yang, B., Chen, C., Habib, A., 2019. NRLI-UAV: non-rigid registration of sequential raw laser scans and images for low-cost UAV LiDAR point cloud quality improvement. ISPRS J. Photogrammetry Remote Sens. 158, 123–145.

Liu, X., 2011. Accuracy assessment of LIDAR elevation data using survey marks. Surv. Rev. 43 (319), 80–93. https://doi.org/10.1179/003962611x12894696204704.

Liu, X., Zhang, Z., Peterson, J., Chandra, S.S., 2007. LIDAR-derived high quality ground control information and DEM for image orthorectification. GeoInformatica 11 (1), 37–53. https://doi.org/10.1007/s10707-006-0005-9.

Maas, H.G., 2003. Planimetric and height accuracy of airborne laser scanner data - user requirements and system performance, Proceedings 49 Photogrammetric. Week. D. Fritsch), Wichmann Verlag, pp. 117–125.

Maune, D.F., Maitra, J.B., McKay, E.J., 2007. Accuracy standards & guidelines. In: Maune, D.F. (Ed.), Digital Elevation Model Technologies and Applications: the DEM User's Manual. second ed., American Society for Photogrammetry and Remote Sensing, Bethesda, Maryland, pp. 65–97.

Montane, J.M., Torres, R., 2006. Accuracy assessment of lidar saltmarsh topographic data using RTK GPS. Photogramm. Eng. Rem. Sens. 72 (8), 961–967. https://

doi.org/10.14358/pers.72.8.961.
Mouzakidou, K., Brun, A., Cucci, D.A., et al., 2024. Airborne sensor fusion: expected accuracy and behavior of a concurrent adjustment. ISPRS Open Journal of Photogrammetry and Remote Sensing 100057.
Muhadi, N.A., Abdullah, A.F., Bejo, S.K., Mahadi, M.R., Mijic, A., 2020. The use of LiDAR-derived DEM in flood applications: a review. Rem. Sens. 12, 2308. https://doi.org/10.3390/rs12142308.
NDEP, 2004. Guidelines for digital elevation data. National Digital Elevation Program (NDEP). Version 1.0. http://www.ndep.gov/NDEP_Elevation_Guidelines_Ver1_10May2004.pdf. (Accessed 18 January 2009). Last date accessed.
Pereira, L.G., Janssen, L.L.F., 1999. Suitability of laser data for dtm generation: a case study in the context of road planning and design. ISPRS J. Photogrammetry Remote Sens. 54 (4), 244–253. https://doi.org/10.1016/s0924-2716(99)00018-0.
Pfeifer, N., Briese, C., 2007. Geometrical aspects of airborne laser scanning and terrestrial laser scanning. International Archives of Photogrammetry. Remote Sensing and Spatial Information Sciences 36 (3/W52), 311–319.
Pirasteh, S., Li, J., 2018. Developing an algorithm for automated geometric analysis and classification of landslides incorporating LiDAR-derived DEM. Environ. Earth Sci. 77 (11). https://doi.org/10.1007/s12665-018-7583-3.
Pourali, H., Arrowsmith, C., Chrisman, N., Matkan, A., 2014. Vertical accuracy assessment of LiDAR ground points using minimum distance approach. CEUR Workshop Proceedings 1142, 86–96.
Qi, Z., Li, S., Pang, Y., Du, L., Zhang, H., Li, Z., 2023. Monitoring spatiotemporal variation of individual tree biomass using multitemporal LiDAR data. Rem. Sens. 15, 4768. https://doi.org/10.3390/rs15194768.
Qiao, G., Wang, W., Wu, B., Liu, C., Li, R., 2010. Assessment of geo-positioning capability of high-resolution satellite imagery for densely populated high buildings in metropolitan areas. Photogramm. Eng. Rem. Sens. 76 (8), 923–934. https://doi.org/10.14358/pers.76.8.923.
Renslow, M., 2013. Manual of Airborne Topographic LIDAR.
Reutebuch, S.E., Andersen, H.-E., McGaughey, R.J., 2005. Light detection and ranging (LiDAR): an emerging tool for multiple resource inventory. J. For. 103 (6), 286–292.
Schmelz, W.J., Psuty, N.P., 2019. Quantification of airborne lidar accuracy in coastal dunes (Fire Island, New York). Photogramm. Eng. Rem. Sens. 85 (2), 133–144. https://doi.org/10.14358/pers.85.2.133.
Shan, J., Toth, C.K., 2018. Topographic laser ranging and scanning. https://doi.org/10.1201/9781315154381.
Sheng, Y., Gong, P., Biging, G.S., 2003. True orthoimage production for forested areas from large-scale aerial photographs. Photogramm. Eng. Rem. Sens. 69 (3), 259–266. https://doi.org/10.14358/pers.69.3.259.
Sibson, R., 1981. A brief description of natural neighbor interpolation (Chapter 2). In: Barnett, V. (Ed.), Interpreting Multivariate Data. John Wiley, Chichester, England, pp. 21–36.
Toth, C., 2004. Future trends in LiDAR. In: Proceedings of the ASPRS 2004 Annual Conference. Denver, Colorado, 23–28 May, unpaginated CD-ROM.
Vo, A.V., Laefer, D.F., Bertolotto, M., 2016. Airborne laser scanning data storage and indexing: state-of-the-art review. Int. J. Rem. Sens. 37 (24), 6187–6204. https://doi.org/10.1080/01431161.2016.1256511.
Vosselman, G., Maas, H., 2010. Airborne and Terrestrial Laser Scanning. pp. 19–32.
Vosselman, G., Maas, H.G., 2001. Adjustment and filtering of raw laser altimetry data. In: Proceedings of the OEEPE Workshop on Airborne Laser Scanning and Interferometric SAR for Detailed Digital Terrain Models. Stockholm, Sweden.
Wallace, L., Lucieer, A., Watson, C., Turner, D., 2012. Development of a UAV-LiDAR system with application to forest inventory. Rem. Sens. 4, 1519–1543. https://doi.org/10.3390/rs4061519.
Webster, T., 2005. LIDAR validation using gis: a case study comparison between two LIDAR collection methods. Geocarto Int. 20 (4), 11–19. https://doi.org/10.1080/10106040508542359.
Webster, T., Dias, G.J., 2006. An automated GIS procedure for comparing GPS and proximal LIDAR elevations. Comput. Geosci. 32 (6), 713–726. https://doi.org/10.1016/j.cageo.2005.08.009.
Webster, T., Forbes, D.L., Dickie, S., Shreenan, R., 2004. Using topographic lidar to map flood risk from storm-surge events for charlottetown, prince edward Island, Canada. Can. J. Rem. Sens. 30 (1), 64–76. https://doi.org/10.5589/m03-053.
Wu, B., Tang, S., Zhu, Q., Tong, K.-Y., Han, H., Li, G., 2015. Geometric integration of high-resolution satellite imagery and airborne LiDAR data for improved geopositioning accuracy in metropolitan areas. ISPRS J. Photogrammetry Remote Sens. 109, 139–151. https://doi.org/10.1016/j.isprsjprs.2015.09.006.
Xhardé, R., Long, B.F., Forbes, D.L., 2006. Accuracy and limitations of airborne LiDAR surveys in coastal environments. In: 2006 IEEE International Symposium on Geoscience and Remote Sensing. pp. 2412–2415. https://doi.org/10.1109/IGARSS.2006.625Denver, CO, USA.
Yao, W., Zhang, M., Hinz, S., Stilla, U., 2011. Airborne traffic monitoring in large areas using LiDAR data – theory and experiments. Int. J. Rem. Sens. 33 (12), 3930–3945. https://doi.org/10.1080/01431161.2011.637528.